The Maculalactone Biosynthetic Gene Cluster, a Cryptic Furanolide Pathway Revealed in *Nodularia* sp. NIES-3585

Paul M. D'Agostino,[1,2,¥] Roberta R. de Castro,[1,3,¥] Valdet Uka,[1,4] Kumar Saurav,[5] Tobias M. Milzarek,[1,2] Angela Sester,[1,2] Maria Paula Schneider,[3] Tobias A. M. Gulder[1,2]

[1]Chair of Technical Biochemistry, Technical University of Dresden, Bergstraße 66, 01069 Dresden, Germany

[2]Department of Natural Product Biotechnology, Helmholtz Institute for Pharmaceutical Research Saarland (HIPS), Helmholtz Centre for Infection Research (HZI) and Department of Pharmacy at Saarland University, PharmaScienceHub (PSH), Campus E8.1, 66123, Saarbrücken, Germany.

[3]Laboratory of Genomics and Biotechnology, Federal University of Pará, Av. Augusto Correa 1, 66075-110, Belem-PA, Brazil

[4]Division of Pharmacy, Faculty of Medicine, University of Prishtina, Prishtina, Kosovo

[5]Laboratory of Algal Biotechnology, Centre Algatech, Institute of Microbiology of the Czech Academy of Sciences, Třeboň 379 01, Czech Republic

[¥]Authors contributed equally

Corresponding Author: T.A.M.G: tobias.gulder@helmholtz-hips.de

ORCID

P.M.D: 0000-0002-8323-5416

R.R.C: 0000-0002-8114-9805

V.U: 0000-0003-3141-732X

K.S: 0000-0002-7084-4204

T.M.M: 0000-0001-7512-9093

A.S: 0000-0002-8613-598X

M.P.S: 0000-0002-2538-4827

T.A.M.G: 0000-0001-6013-3161

Keywords: cyanobacteria, natural products, γ-alkylidenebutenolide, furanolides, molecular networking, DiPaC, GNPS

Abstract

Cyanobacteria have long been known as a prolific source of bioactive natural products (NPs). One such group of NPs are the furanolides, whose first congeners were discovered in the 1980's and 1990's. A structural characteristic of furanolides is a γ-butyrolactone moiety with aromatic or aliphatic substituents at the α- and β-positions and an aromatic substituent at its γ-position. Recent elucidation of the genetic basis of furanolide formation enables a genome mining approaches to discover related cryptic furanolide biosynthetic gene clusters (BGCs).

Within this work, a cryptic BGC (15.5 kb) from *Nodularia* sp. NIES-3585 was cloned using the Direct Pathway Cloning (DiPaC) strategy and heterologously expressed in *E. coli* BAP1. Isolation and structural elucidation of the major recombinant products led to the discovery of the known furanolide maculalactone B and the new analogue maculalactone N. Both compounds possess potent antibiotic activity against both gram-positive and gram-negative bacteria.

To identify related maculalactone-like structures, Global Natural Product Social Molecular Networking (GNPS) analysis of high-resolution LCMS data was applied. This led to the identification of 20 maculalactone-related molecules. Structural analysis based on manual annotation of MS/MS fragment ions suggest the maculalactones to strictly possess phenolic α- and γ-substituents with various hydroxylation patterns whilst the β-substituent appears highly variable and may contain a phenolic, aliphatic, or indole portion. Additionally, several structural analogues contain a furan-ring hydroxylation.

These results show the flexibility of the maculalactone core-forming enzymes to utilise various substrates resulting in considerable structural diversity and highlight DiPaC as an efficient strategy to discover the encoded products of cyanobacterial cryptic BGCs.

1. Introduction

Cyanobacteria have long been known as producers of structurally intriguing bioactive natural products (NPs).[1,2] One class of NPs found in cyanobacteria are the furanolides containing a γ-butyrolactone core structure (**1**) with aromatic or aliphatic substituents at the α- and β-positions, and a conserved aromatic substituent at the γ-position (Figure 1). Cyanobacterial furanolides include the potent phytotoxin cyanobacterin (**2**),[3,4] the first chlorinated NP discovered from a freshwater cyanobacterium, the nostoclides (e.g. **3**),[5,6] and the maculalactones (e.g. **4**-**5**).[7–9]

The maculalactones were exclusively isolated from the marine cyanobacterium *Kyrtuthrix maculans*, collected from rocks at several locations along Hong Kong's shores.[8–11] To date, the maculalactones are the largest and most structurally complex sub-group of furanolides consisting of approximately 14 NPs and exhibiting diverse features including tribenzyl- (e.g. **4**) or dibenzyldiphenyl variants (e.g. **5**), with all substituents on the maculalactone core moiety being aromatic (Figure 1).[8–12] The (+)-maculalactone A ((*S*)-enantiomer) is the major compound present in *K. maculans*, and (±)-maculalactone A (**4**) was shown to possess antifouling activity against marine herbivores and marine settlers.[7]

Our group recently provided key insights into furanolide biosynthesis by identifying and characterising the cyanobacterin (*cyb*) biosynthetic gene cluster (BGC).[13] Biosynthesis occurs by forming the first *C-C* bond by an acyloin condensation reaction utilising two α-keto acids catalysed by the thiamine pyrophosphate-dependent (TPP) enzyme CybE. Next, coumaroyl-CoA is formed from deamination of tyrosine by the ammonia lyase CybB, followed by its CoA-activation by the CoA-ligase CybC. The furanolide synthase CybF catalyses a cascade to fuse the acyloin intermediate with the resulting coumaroyl-CoA, involving decarboxylative *O*-acylation followed by a Morita–Baylis–Hillman (MBH) reaction and a final 1,4-hydride shift that facilitates late-stage adjustment of oxidative states, resulting in two more *C-C* bonds and formation of the γ-butyrolactone, common across the furanolide family of NPs.[13]

During our ongoing identification of cryptic furanolide BGCs throughout cyanobacteria, comparative genomics of *Nodularia* sp. NIES-3585 revealed a cryptic furanolide BGC encoding all four critical γ-butyrolactone forming enzymes yet in a distinct genomic neighbourhood. Enabled by our Direct Pathway Cloning (DiPaC)[13–22] strategy for BGC capture and expression, this BGC was investigated using heterologous expression. Herein, we detail the comprehensive characterisation of this BGC from *Nodularia* sp. NIES-3585 through integrated molecular, biochemical, and analytical approaches, leading to the discovery of the maculalactone (*mac*) BGC, elucidation of a novel furanolide structure, and the identification of multiple new maculalactones based on molecular networking and MS/MS fragmentation data.

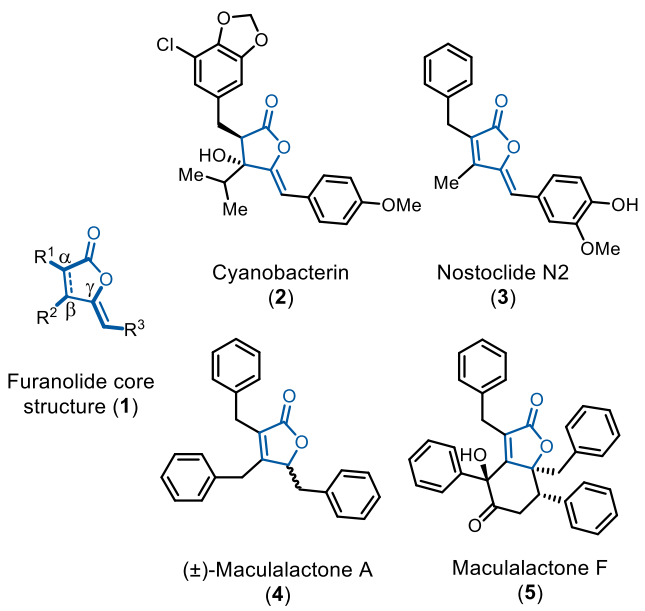

Figure 1: Cyanobacterial furanolides. The γ-butyrolactone core moiety (**1**, blue) is consistent across the majority of furanolides. The α- and β-positions (R^1 and R^2, respectively) consist of an aliphatic or aromatic substituent whilst the γ-position (R^3) is an aromatic substituent. Members of the furanolides include cyanobacterin (**2**), nostoclide N2 (**3**), and the maculalactones, with analogues such as the (±)-maculalactone A (**4**) and F (**5**).

2. Results and Discussion

2.1 Bioinformatic Analysis

The core cyanobacterin biosynthetic sequences of the proteins CybBCEF were used to screen for candidate furanolide BGCs within the genome of *Nodularia* sp. NIES-3585. A region spanning approximately 15.5 kb in length and consisting of 11 genes was identified (Figure 2A; Supporting Table S1). The respective BGC encoded all four core furanolide biosynthetic genes consistent with *cyb* and nostoclide N (*ncl*) BGCs, as well as other anticipated genes involved in precursor supply.[5,13] These include 3-deoxy-D-arabinoheptulosonate 7-phosphate (DAHP) synthase (*macA*) and chorismate mutase (*macM*) – both involved in biosynthesis of aromatic amino acids – and a tyrosinase (*macK*), predicted to perform *ortho* hydroxylation of tyrosine. Additionally, there are several open reading frames that putatively belong to the *mac* BGC but for which a function has not been predicted, including genes encoding two hypothetical proteins (*orf1* and *orf2*), a NADH-flavin reductase (*orf3*) and a phycocyanobilin:ferredoxin oxidoreductase (*orf4*). The overall composition of the identified candidate BGC strongly indicated its function in furanolide biosynthetic assembly.

2.2 Heterologous Expression and NP Structure Elucidation

To experimentally link the cryptic BGC with its encoded products and to investigate potential roles of additional genes of which no homologs are found in the *cyb* pathway, two separate expression plasmids were constructed (Figure 2A and 2B). The first construct, pET28b-ptetO::*mac*, incorporated the entire BGC in its native arrangement while the second construct, pET28b-ptetO::*macBCEF*, contained only the four core furanolide biosynthetic genes. Following heterologous expression of both plasmids in *E. coli* BAP1, HPLC analysis revealed the production of several new compounds from the pET28b-ptetO::*mac* and pET28b-ptetO::*macBCEF* expressions (Figure 2C). However, no differences between the two expression constructs were observed. To comprehensively explore the metabolome of both expression strains compared to the control, HRMS-based secondary analysis was performed using PCA and PLS-DA multivariate analyses.[23,24] Both score plots showed a clear separation in PC1 (Principal Component 1) for the expression plasmids when compared to the control, while PC2 revealed minor differences between both expression plasmids. The analysis thus indicated that while the respective metabolomes of the two BGC expression strains were only slightly distinct from each other, they differed substantially from those using only the vector backbone as a control (Supporting Figure S1-S4).

Isolation of the two major products was performed using semi-preparative HPLC. LC-HRMS of the isolated peaks revealed an *m/z* 353.1536 $[M+H]^+$ and 369.1484 $[M+H]^+$ with calculated chemical formulae of $C_{25}H_{20}O_2$ and $C_{25}H_{20}O_3$ for compounds **6** and **7**, respectively. Submission of both isolated compounds to ^1H and ^{13}C NMR confirmed the presence of 25 carbons, including a characteristic ester signal (δ_C 170.5; 170.6) and at least two aromatic phenyl systems in broad agreement with the maculalactone NP family.[10,12] Compound **6** was confirmed to be maculalactone B and identified as a mixture of interconverting (*E/Z*)-isomers at positions C4 and C1^c (Figure 2D). The NMR data of compound **7** was highly similar to those of **6**, containing almost identical aromatic substituents. The higher mass (+16 u), corresponding to a single oxygen and the occurrence of typical aromatic signals (δ_C 154.7; δ_H 6.97 (d, 8.5), 6.75 (d, 8.6)) indicated one aromatic residue to be a 4-hydroxyphenol moiety. The position of the hydroxy group was deduced from HMBC correlations from C4^a to C1^a and C1^a to C3 and thus located on the phenol in the furanolide α-position, therefore likely being derived from incorporation of 4-coumaryl-CoA instead of cinnamoyl-CoA. This is the first report of this NP and the compound was named maculalactone N (**7**).

2.3 Antibacterial Activities of Maculalactones B (6) and N (7)

Compounds **6** and **7** exhibited selective antimicrobial activity against several tested bacteria (Supporting Table S2). Against gram-negative bacteria, **7** demonstrated high potency, with MIC values of 0.195 µg/mL against *E. coli* CCM2024 and 0.390 µg/mL against *Pseudomonas aeruginosa* CCM1959, while **6** showed moderate activity against *E. coli* CCM2024 (MIC 3.125 µg/mL). Their activity against gram-positive bacteria was notably lower, with only modest inhibition of *Bacillus subtilis* (MIC 100 and 25 µg/mL for **6** and **7**, respectively) and undetectable activity against the pathogenic strains *Staphylococcus aureus* CCM3824 and

Streptococcus sanguinis CCM4047. These results indicate a specific antimicrobial activity against the selected gram-negative facultative pathogens and provide a foundation for future studies investigating the relationship between hydroxyl-substitution patterns and antimicrobial activity.

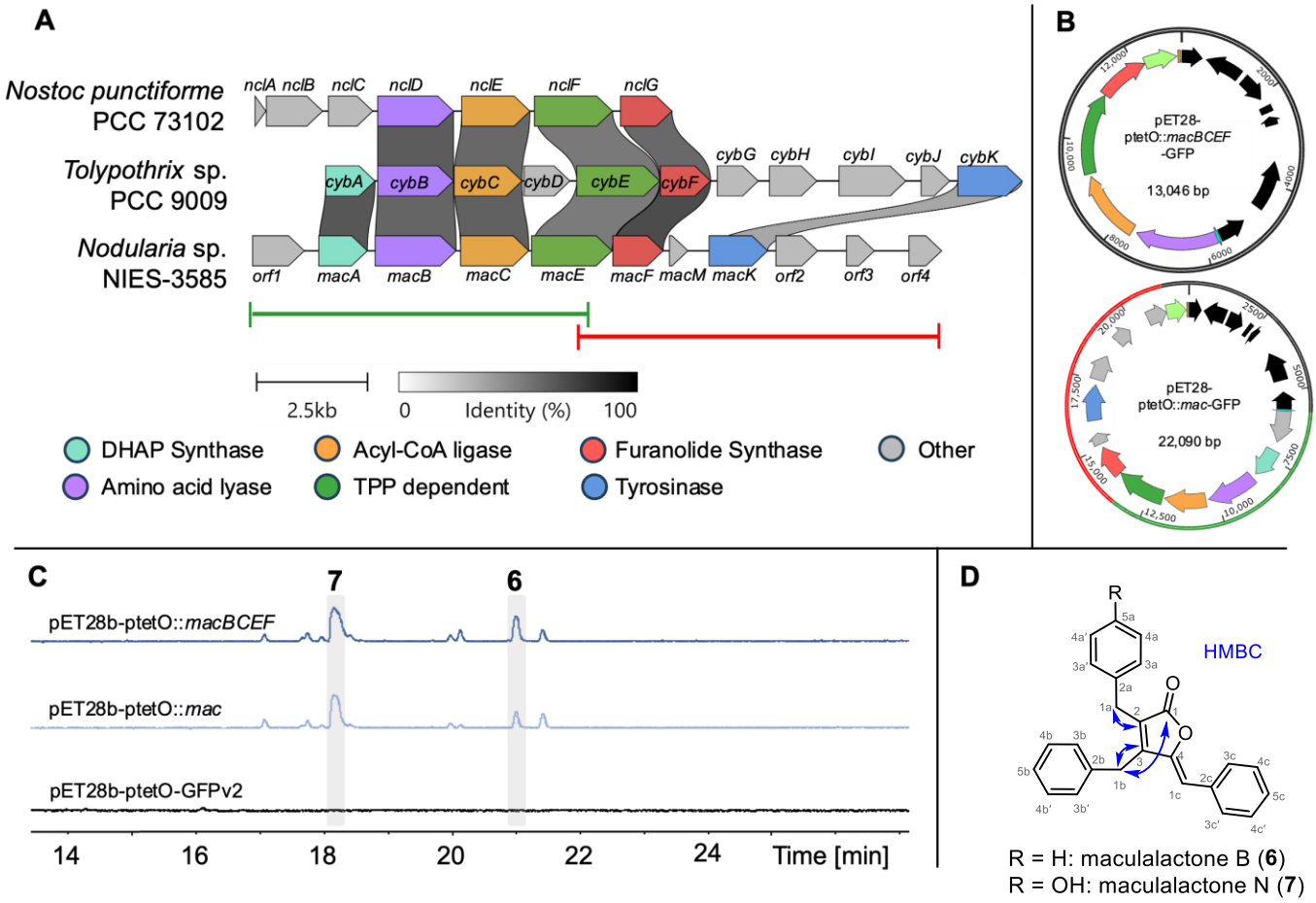

Figure 2: The maculalactone (*mac*) BGC and isolated NPs. A) BGC comparison of *mac* with the *cyb* and *ncl* BGCs. Green and red lines indicate design of PCR products used for BGC DNA amplification and downstream assembly. **B)** pET28-ptetO::*macBCEF* and pET28-ptetO::*mac* plasmid maps. **C)** HPLC-UV (330 nm) chromatogram comparing extracts from the two expression plasmids to the empty expression vector control. The two compounds selected for isolation are highlighted in grey. **D)** Structures and selected decisive HMBC correlations (blue arrows) used for structure elucidation of the two isolated maculalactones **6** and **7** (for full NMR data, cf. Supporting Table S3 and Supporting Figures S18-S27).

2.4 Molecular Networking and Identification of Further Maculalactone Analogues

In addition to the maculalactones **6** and **7** isolated and characterised above, several new products were detected in BGC versus empty-control expression experiments, albeit at very low abundance. To identify the respective compounds, a LC-HRMS/MS GNPS molecular networking approach was performed (Supporting Figure S5). GNPS identified a small network of nodes that included the parent ions of **6** and **7**, suggesting shared fragmentation patterns of the maculalactone sub-group of furanolides (Figure 3). Extensive MS/MS annotation of fragment ions resulted in the designation of a further 18 maculalactone-related NPs (Table 1, **8**-**17**, Supporting Figure S6-S17) including the predicted maculalactone precursors

kurasoin A/B[25] (**16**) and cinnamic acid (**17**). Furanolides are commonly observed as *E*/*Z* isomeric pairs (**a**/**b**) due to isomerisation of the double bond (C4-C1[c]) located at the γ-position of the furanolide core. Maculalactones were no exception with the identification of *E*- and *Z*-isomers observed in almost all cases, where the latter was the major compound as expected from previous observations (Figure 3B).[6,13]

Maculalactones with phenolic substituents at the α-, β- and γ-positions were identified as the major NPs, indicating substrate preferences of the maculalactone core biosynthetic enzymes. Tri-phenolic maculalactones were identified with varying hydroxylation patterns and were either non- (**6a/b**), mono- (**7a/b**), or di-hydroxylated (**8a/b**, **9**). Among the di-hydroxylated variants, two structural types exist: compounds **8a/b** with two single hydroxylations on distinct phenols and compound **9**, with two hydroxylations on the same phenol.

Other structurally distinct maculalactones include those with a phenolic α- and γ-substituent and an aliphatic or indole β-substituent. Compounds **10a/b** (*m*/*z* 319.1692 $[M+H]^+$; $C_{22}H_{23}O_2$) correspond to the potential incorporation of 4-methyl-2-oxopentanoic acid (derived from leucine) or 3-methyl-2-oxopentanoic acid (derived from isoleucine). Similar substituents were observed in *E. coli* extracts and *in vitro* assays of cyanobacterin biosynthetic enzymes but a clear preference for 3-methyl-2-oxopentanoic acid was reported.[13] The β-substituent showed further flexibility, with compounds **11a/b** (*m*/*z* 392.1645 $[M+H]^+$; $C_{27}H_{22}NO_2$) and **12a/b** (*m*/*z* 408.1595 $[M+H]^+$; $C_{27}H_{22}NO_3$) having an indole substituent, making these the first reported furanolides to contain a nitrogen atom.

The third group of NPs identified contained a furanolide ring hydroxylation, most likely at the α- or β-position. The presence of the furan hydroxylation compared to phenolic hydroxylation is implied by the strong loss of H_2O observed by the ion $[M+H-H_2O]^+$. This includes ring hydroxylation of **6a/b**, **7a/b** and **10a/b** corresponding to the known NP maculalactone L (**13**), as well as **14a/b**, and **15a/b**, respectively. Maculalactone L has an α-hydroxylation whilst cyanobacterin, the only other furan hydroxylated furanolide reported, is β-hydroxylated.[3,8] So far, the origin of the hydroxyl group remains elusive but our results revealed that **13**-**15** were produced by the full and minimal (*macBCEF*) expression vectors (Figure 3B).

Maculalactones produced by *K. maculans* structurally fall into two broad categories: the tribenzylbutyrolactones (e.g. maculalactone N; **7**), and the dibenzyldiphenyl-4,5,6,7-tetrahydrobenzofuranones, characterized by a six-membered carbocycle and diverse hydroxylations (e.g. maculalactone F; **5**).[10,12] However, we were unable to detect any of the dibenzyldiphenyl-4,5,6,7-tetrahydrobenzofuranones in our *E. coli* heterologous extracts and despite extensive screening, no maculalactone-related NPs could be identified in either the cell pellet or supernatant of the *Nodularia* sp. NIES-3585 native producer under laboratory growth conditions, suggesting that the *mac* BGC is silent under these conditions. Genetic analysis of the *mac* BGC did not reveal putative genes responsible for the complex dibenzyldiphenyl-4,5,6,7-tetrahydrobenzofuranone formation and thus, biosynthesis of these structurally intriguing maculalactones remains unsolved. Based on data obtained in this study, we therefore hypothesise that the *Nodularia* sp. NIES-3585 *mac* BGC is distinct from the one encoded in *K. maculans*.

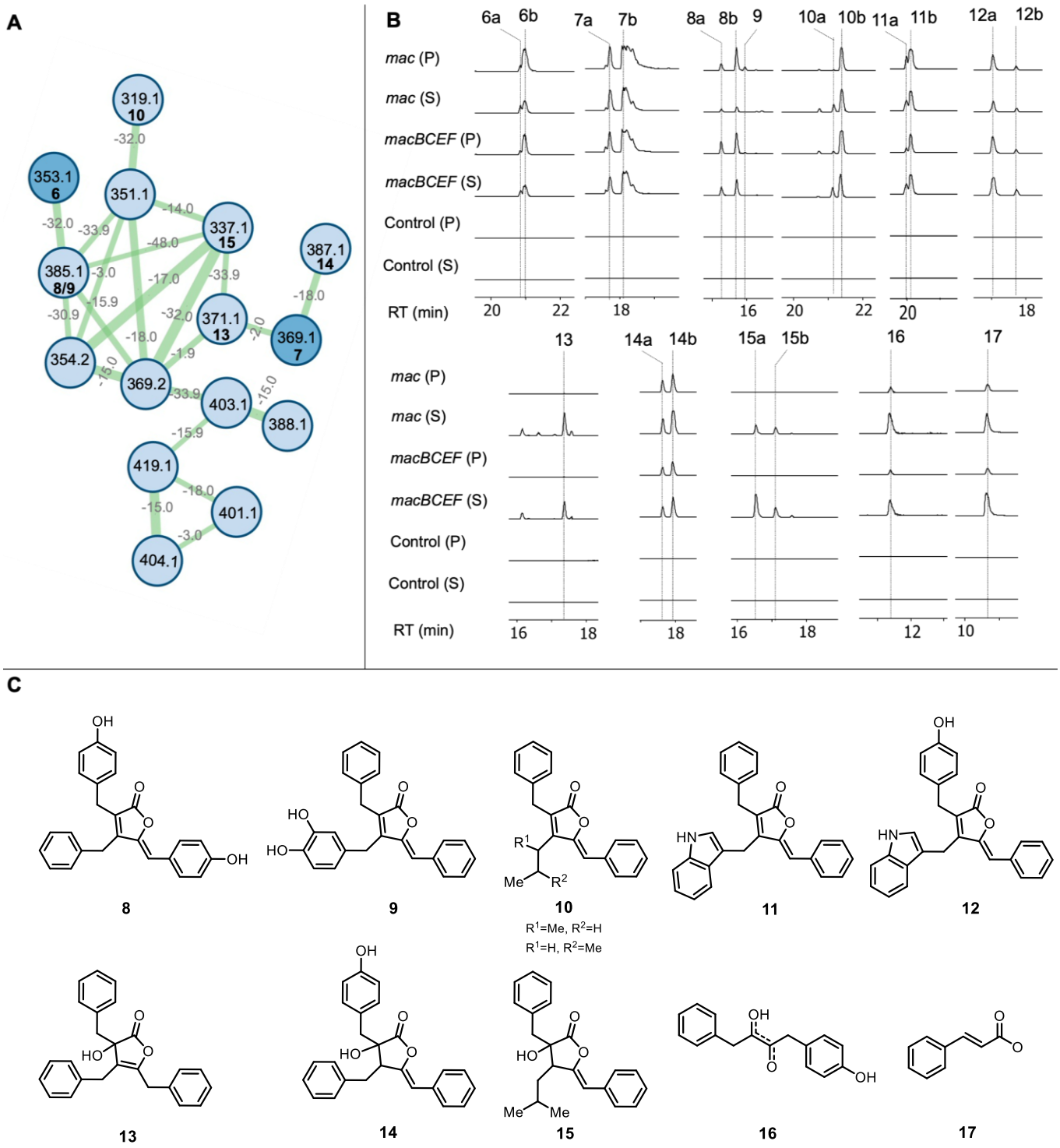

Figure 3: Additional maculalactone analogues identified by GNPS. A) A molecular network of the maculalactone NPs created using the online workflow on the GNPS website (http://gnps.ucsd.edu) and visualized in Cytoscape 3.9.1. Each node represents a parent mass, edges are labelled with the mass difference between metabolites whereas edge thickness is proportional to the cosine similarity score (>0.7). Dark blue nodes indicate structurally elucidated compounds **6** and **7**. **B)** Extracted ion chromatograms (EICs): **6a/b** (353.15); **7a/b** (369.14); **8a/b**, **9** (385.14); **10a/b** (319.16); **11a/b** (392.16); **12a/b** (408.16); **13** (371.16); **14a/b** (387.16); **15a/b** (337.18); **16** (257.11); **17** (149.06). All EICs per each panel are depicted in fixed intensity scale. **C)** Structures based on analysis of MS/MS fragmentation patterns. All structures are depicted and HRMS/MS spectra of all maculalactone-related NPs are fully annotated (Figures S6-S17).

Table 1: List of is isolated and MS/MS predicted compounds

Compound	RT (min)	Measured *m/z* $[M+H]^+$	Error (ppm)	Formula
maculalactone C (**6a**)	20.9	353.1536	0.1	$C_{25}H_{21}O_2$
maculalactone B (**6b**)	21.1			
7a	17.7	369.1484	0.3	$C_{25}H_{21}O_3$
maculalactone N (**7b**)	18.1			
8a	15.3	385.1434	0.1	$C_{25}H_{21}O_4$
8b	15.7			
9	15.9			
10a	21.2	319.1692	0.3	$C_{22}H_{23}O_2$
10b	21.4			
11a	20.0	392.1645	0.6	$C_{27}H_{22}NO_2$
11b	20.3			
12a	17.1	408.1595	-0.3	$C_{27}H_{22}NO_3$
12b	17.7			
maculalactone L (**13**)	17.4	371.1642	0.0	$C_{25}H_{23}O_3$
14a	17.7	387.1590	0.2	$C_{25}H_{23}O_4$
14b	17.9			
15a	16.5	337.1803	-1.3	$C_{22}H_{25}O_3$
15b	17.1			
kurasoin A/B (**16**)	11.4	257.1182	-4.0	$C_{16}H_{17}O_3$
cinnamic acid (**17**)	10.6	149.0597	-0.2	$C_9H_9O_2$

3 Conclusion

Furanolides are a class of γ-alkylidenebutenolide NPs with significant structural and bioactive diversity. This work represents the first comprehensive characterisation of the *mac* BGC, providing crucial insights into the genetic basis of maculalactone biosynthesis and expanding our understanding of furanolide diversity in cyanobacteria. Employing the DiPaC strategy, we successfully accessed a silent BGC from *Nodularia* sp. NIES-3585, the products of which would have remained undetectable under standard laboratory growth conditions. By heterologously expressing the cryptic furanolide BGC, we enabled the isolation of the known maculalactone B (**6**) and discovered the new maculalactone N (**7**), which both possess considerable antimicrobial activity. The detection of antibacterial activity in **6** and **7** expands the reported biological activities of the maculalactone family, suggesting these molecules may have evolved diverse defensive functions.

The subsequent GNPS analysis enlarges known maculalactone structural variations, identifying a comprehensive set of 20 maculalactone-related NPs produced by the *mac* BGC. This study not only extends the known chemical space of furanolides but also demonstrates the power of genome mining and heterologous expression techniques to uncover cryptic cyanobacterial biosynthetic potential. Our study revealed a consistent pattern of phenolic substitution at the α- and γ-positions, while demonstrating remarkable flexibility in the β-substituent, which can accommodate phenolic, indole, or aliphatic substituents. The potential for furan-ring hydroxylation further highlights the structural plasticity of these NPs. Thus, our findings underscore the enzymatic versatility of the maculalactone biosynthetic pathway and provide a potential avenue for biocatalytic production of structurally diverse unnatural furanolides.

4 Materials and Methods

4.1 Bacterial Strains, Plasmids, and Genomic DNA Extraction

Nodularia sp. NIES-3585 was purchased from the Japanese Microbial Culture Collection at the National Institute for Environmental Studies (https://mcc.nies.go.jp). The strain was cultured in static batch cultures in BG-11 medium, pH 8 (Sigma-Aldrich, Germany), at room temperature under natural light conditions. Biomass was harvested by centrifugation (4,000*g*, 30 min, 4°C) and frozen at -80°C. Genomic DNA was obtained

using an optimized method for cyanobacteria as previously described.[13,14] Supporting Table S4 summarizes the bacterial strains and plasmids used and generated in this study.

4.2 Direct Pathway Cloning

Putative furanolide biosynthetic genes in *Nodularia* sp. NIES-3585 were identified using the *cyb* CybBCEF protein sequences (GenBank accession number BK059219) as a query. Prior to initiating cloning experiments, the intergenic regions of the 15.5 kb *mac* cluster were analysed for potential *E. coli* transcriptional terminators using ARNold,[26] but no such sequences were identified. Subsequently, primers were designed for targeting the complete predicted *mac* BGC and the minimal *macBCEF* with 20-25 bp homology overlaps at terminal target regions (Supporting Table S5). Attempts to amplify the entire *mac* BGC in one fragment failed, so insert amplification was performed in two fragments (

Figure A). The vector backbone (pET28b-ptetO-GFPv2) was amplified as a linear nucleotide sequence by PCR using previously described primers.[16] Amplifications were performed in 50 µL reactions using Q5 High-Fidelity DNA polymerase (NEB). Reaction setup and thermocycling conditions were performed according to the manufacturer's guidelines. For primers containing a homology arm, the best annealing temperatures were evaluated by performing a temperature gradient between 50-65 °C whilst the annealing temperatures for specific primers were calculated using the NEB Tm Calculator (https://tmcalculator.neb.com). The linearized vector was treated with DpnI (37°C, 3 h; 65°C, 20 min) to remove template plasmid DNA.

All DNA fragments were purified directly on column using the Monarch® PCR & DNA Cleanup Kit (NEB), as PCR reactions yielded specific products. For the construction of pET28b-ptetO::*mac* and pET28b-ptetO::*macBCEF*, the purified DNA fragments (0.02-0.5 pmol each) were assembled using either Sequence and Ligation Independent Cloning (SLIC) or HiFi DNA Assembly Cloning Kit (NEB).[14,15] SLIC assembly was performed in a 10 µL reaction using NEBuffer 2.1 and T4 DNA polymerase (NEB), followed by incubation for 45 s at room temperature and 10 min on ice. HiFi assembly was performed according to the manufacturer's guidelines, except for the reaction being performed in a 10 µL final volume. For both assembly strategies, half of the DNA assembly reaction (5 µL) was transformed into chemically competent *E. coli* DH5α or *E. coli* DH10β . Positive clones were identified by colony PCR and sequences verified by restriction digest analysis (ScaI/SspI double digest for pET28b-ptetO::*mac*; DraIII for pET28b-ptetO::*macBCEF*). In addition, the sequences were validated by whole-plasmid sequencing using Oxford Nanopore technology (Eurofins).

4.3 Heterologous expression

Each expression experiment was compared to a simultaneous experiment with *E. coli* BAP1 harbouring the pET28b-ptetO-GFPv2 empty vector, which served as the negative control. A single colony of *E. coli* BAP1 was used to inoculate a 10 mL pre-expression culture grown in LB medium supplemented with 50 µg/mL kanamycin for plasmid selection. The pre-culture was incubated overnight at 30°C with shaking at 200 rpm. The expression cultures for initial verification of recombinant production of new NPs were then inoculated with 1% (v/v) of the pre-expression cultures in 200-400 mL of M9, LB, and TB medium supplemented with 50 µg/mL kanamycin. Incubation was conducted at 37°C with shaking at 200 rpm until an OD_{600} of 0.4 (M9), 0.6 (LB) or 1.0 (TB) was reached. Cultures were then cooled on ice for >1 hour, induced with 0.5 µg/mL tetracycline, and incubated for 5 days at 20°C with shaking at 200 rpm protected from light. Larger expression cultures for compound isolation and characterization were prepared as above, with 1 L fermentation volume using TB medium for optimal expression.

4.4 Extraction and analysis by HPLC

E. coli biomass was harvested by centrifugation (10,000*g* for 10 min). The supernatant was transferred to a separating funnel and extracted three times with identical volume of ethyl acetate. The cell biomass was extracted using methanol with simultaneous mechanical cell disruption in a sonicator bath for 30 min. Extracted cell debris was removed by centrifugation (10,000*g* for 10 min). Solvents from both extractions were removed *in vacuo* at 40°C using a rotary evaporator. Desiccated extracts were dissolved in 500 µL HPLC-grade methanol and the resulting solution filtered through a Millex-GP 0.22 µm PES syringe membrane filter (Millipore, USA) prior to injection into HPLC and HPLC-MS systems. *Nodularia* sp.

NIES-3585 biomass was collected as a dense culture after one month of growth. Cyanobacterial biomass was centrifuged at 12,000*g* for 30 min to separate the pellet and supernatant. Each fraction was then extracted as described above for *E. coli*.

Analytical HPLC was performed on a Knauer Azura system. Chromatographic separation was performed at 25°C on a Eurosphere II 100-3 C18 A (150 × 4.6 mm) column with integrated precolumn manufactured by Knauer. A wavelength of 220 nm was used for detection and a PDA UV spectrum covering 200-600 nm recorded over the entire run. Eluents used for chromatographic separation were water (A) and acetonitrile (B), both supplemented with 0.05% trifluoracetic acid. The gradient was set as follows: Preconditioning 5% B; 0–2 min: 5% B, 2-30 min: 5-100% B, 30-35 min: 100% B, 35-38 min: 100-5% B, at a constant flow rate of 1 mL/min.

4.5 Liquid Chromatography-High Resolution Mass Spectrometry (LC-HRMS)

The LC-HRMS experiments were carried out using an Impact II (Bruker Daltonics GmBH & Co. KG) quadrupole time-of-flight (qTOF MS) instrument equipped with an electrospray ionization source (ESI, Apollo II) coupled to an Elute UHPLC 1300 system (Bruker). An Intensity Solo C18 (1.8 µm, 2.1 mm, 100 mm) from Bruker Daltonics was used for separation. The mobile phases consisted of water (100%) containing 0.1% formic acid (solvent A) and acetonitrile (100%) containing 0.1% formic acid (solvent B). The following gradient was applied: 0–2 min: 5% B, 2–25 min; 5%–95% B, 25–28 min; 95% B, 28–30 min; 5% B. The flow rate was 0.3 mL/min and the column temperature was set at 40°C. The ESI source was also connected to an external syringe pump (Hamilton syringe 2.5 mL) for pre-acquisition calibration and was operated in the positive ESI mode (ESI+). The external syringe pump was used for mass calibration using a Na-Formate calibrant solution (Na-Formate cluster: 12.5 mL H_2O, 12.5 mL isopropanol, 50 µL formic acid conc., 250 µL NaOH 1M). The syringe pump injects the calibration solution matching the polarity of ionization and calibrates the mass axis of the Impact II system in all scan functions used (MS and/or MS/MS). The Q-TOF HRMS method consisted of a full scan TOF survey (50–1300 Da) and a maximum number of three DDA MS/MS scans. The source parameters were as follows: Dry gas 8 L/min, nebulizer gas 1.8 bar, capillary voltage 4.5 kV and end plate voltage of 500 V. For the DDA MS/MS experiments, a collision energy (CE) ramp of 20-50 V was applied. The instrument was controlled by Hystar and Otof Control software, while data processing and metabolomic analyses were carried out using Data Analysis (Version 6.1) and MetaboScape (Version 8.0.2) software (Bruker).

Principal Component Analysis (PCA) and Partial Least Square Discriminant Analysis (PLS-DA) analyses were performed in the MetaboScape software using the following parameters: Feature detection (peak picking) and alignment was done using the T-Rex 3D algorithm provided within MetaboScape with an intensity threshold of 1500 counts and a minimal peak length of 8 data points. For gap filling, the Recursive Feature Extraction algorithm was enabled. Ion deconvolution and de-adducting was performed by incorporating the most common adducts in positive mode ($M+H^+$, $M+Na^+$, $M+K^+$, $M-H_2O+H^+$, $M-2H_2O+H^+$). For computing the final PCA and PLS-DA plots, data were scaled using Pareto scaling.[23,24]

4.6 GNPS Molecular Networking

All HRMS data files (*.d* format) were converted to the open data format *.mzML* using the MSConvert software from ProteoWizard.[27] The converted files were uploaded to the Global Natural Product Social (GNPS) environment, where a classical molecular networking method was generated using the online workflow (http://gnps.ucsd.edu).[28] MS/MS spectra underwent window-filtering by retaining only the top six fragment ions within the +/- 50Da window across the spectrum. The mass tolerance was set to 0.02 Da for both precursor ions and MS/MS fragment ions. A network was constructed with edges filtered according to two criteria: a cosine score threshold above 0.7 and a minimum of five matched peaks. A connection between two nodes was kept only if both nodes ranked among each other's top 10 most similar matches. Molecular families were limited to a maximum size of 100 nodes, with the lowest-scoring edges removed iteratively until this threshold was met. Networks were then compared against GNPS spectral libraries, with library spectra filtered using identical parameters as for the input data. Network visualization and analysis were performed using Cytoscape 3.9.1.[29]

4.7 Isolation of NPs by Semi-Preparative HPLC

Isolation of **6** and **7** was performed on a semi-preparative HPLC controlled by a Jasco HPLC system consisting of an UV-1575 Intelligent UV/VIS Detector, two PU-2068 Intelligent prep. Pumps, a MIKA 1000 Dynamic Mixing Chamber (1000 µL Portmann Instruments AG Biel-Benken), a LC-NetII/ADC, and a Rheodyne injection valve. The system was controlled by the Galaxie-Software. Chromatographic separation was performed on a Eurosphere II 100-5 C18 A (250 x 16 mm) column with precolumn (30 x 16 mm) provided by Knauer and the eluents used were water (A) and acetonitrile (B), both supplemented with 0.05% trifluoracetic acid. The separation method was as follows: Preconditioning 5% B; 0-2 min; 5% B, 2-24min; 5-60% B, 24-34min; 60-70% B, 34-35min; 70-100% B,35-40min; 100% B, re-equilibration at 5% B for 7 minutes and at a constant flow rate of 10 mL/min. Fractions were pooled and dried *in vacuo* before NMR analysis.

4.8 Determination of Antibacterial Activity

Isolated NP **6** and **7** were tested against five bacterial isolates (Supporting Table S2), using the standard broth two-fold microdilution method following the CLSI M100-S20 protocol as previously described.[30] Briefly, each NP was serially diluted in Mueller-Hinton broth to concentrations ranging from 100 to 0.09 µg/mL using 96-well plates. An inoculum from overnight cultures of the test strains was added to each well to achieve a final concentration of approximately 5×10^5 CFU/mL. After adding 0.1 mL culture to each well, the plates were incubated aerobically at 37°C for 16 hours. The minimum inhibitory concentration (MIC) was determined as the lowest concentration of each NP that inhibited microbial growth. Negative controls were prepared using sterile Mueller-Hinton broth and methanol (the dissolving solvent). Erythromycin (32–0.0625 µg/mL) was the positive control for *S. aureus*, and *S. sanguinis*, while gentamicin (32–0.0625 µg/mL) was the positive control for *B. subtilis, E. coli*, and *P. aeruginosa*. Positive controls were dissolved and prepared similarly to the test compounds. The experiments were performed in triplicates.

4.9 NMR Analysis

NMR spectra were recorded on a Bruker AV-500 and a Bruker AV-600 spectrometer at 298 K. The chemical shifts are given in δ-values (pm) and are calibrated on the residual peak of the deuterated solvent ($CDCl_3$: δ_H = 7.26 ppm, δ_C = 77.0 ppm). The coupling constants *J* are given in Hertz [Hz]. The following abbreviations were used for the allocation of signal multiplicities: s – singlet, d – doublet, t – triplet, m – multiplet.

Maculalactone B (6): Isolated as a yellow solid. Analytical data in agreement with literature values.[10,12] **^{1}H-NMR** (500 MHz, $CDCl_3$): δ = 7.71 (d, *J* = 7.3 Hz, 2 H), 7.35 (t, *J* = 7.5 Hz, 2 H), 7.31–7.26 (m, 4 H), 7.26–7.23 (m, 3 H), 7.20–7.17 (m, 2 H), 7.12 (d, *J* = 7.0 Hz, 2 H), 5.98 (s, 1 H), 3.93 (s, 2 H), 3.74 (s, 2 H). **^{13}C-NMR** (125 MHz, $CDCl_3$): δ = 170.5, 150.9, 148.3, 137.6, 136.7, 133.1, 130.6, 129.1, 128.9, 128.8, 128.7, 128.3, 128.0, 127.2, 126.8, 110.6, 30.7, 29.9. **HRMS** (ESI-TOF) *m/z*: $[M+H]^+$ calculated for $C_{25}H_{21}O_2$ 353.1542, found 353.1536; $[M+Na]^+$ calculated for $C_{25}H_{20}NaO_2$ 375.1361, found 375.1356.

Maculalactone N (7): Isolated as a yellow solid. **^{1}H-NMR** (500 MHz, $CDCl_3$): δ = 7.71 (d, *J* = 7.3 Hz, 2 H), 7.35 (t, *J* = 7.5 Hz, 2 H), 7.31–7.26 (m, 2 H), 7.25 (t, *J* = 7.2 Hz, 2 H), 7.20–7.17 (m, 2 H), 6.97 (d, *J* = 8.5 Hz, 2 H), 6.75 (d, *J* = 8.6 Hz, 2 H), 5.98 (s, 1 H), 3.86 (s, 2 H), 3.73 (s, 2 H). **^{13}C-NMR** (125 MHz, $CDCl_3$): δ = 170.6, 154.7, 151.4, 148.3, 137.6, 133.1, 130.6, 129.5, 129.0, 128.9, 128.82, 128.77, 128.7, 127.7, 126.8, 115.9, 110.7, 29.89, 29.86. **HRMS** (ESI-TOF) *m/z*: $[M+H]^+$ calculated for $C_{25}H_{21}O_3$ 369.1491, found 369.1502; $[M+Na]^+$ calculated for $C_{25}H_{20}NaO_3$ 391.1310, found 391.1294.

4.10 Data Availability

The genome of *Nodularia* sp. NIES-3585 is publicly available in NCBI (accession: BDUB00000000).[31] The *mac* BGC, pET28b-ptetO::*mac* and pET28b-ptetO::*macBCEF* sequences were submitted to NCBI (accession: BK070015, PV097226 and PV097227, respectively). MS data is available on the MassIVE GNPS repository (accession: MSV000097078).

5. References

1 M. Baunach, A. Guljamow, M. Miguel-Gordo and E. Dittmann, *Nat. Prod. Rep.*, 2023, **41**, 347–369.
2 M. R. Jones, E. Pinto, M. A. Torres, F. Dörr, H. Mazur-Marzec, K. Szubert, L. Tartaglione, C. Dell'Aversano, C. O. Miles, D. G. Beach, P. McCarron, K. Sivonen, D. P. Fewer, J. Jokela and E. M.-L. Janssen, *Water Res.*, 2021, **196**, 117017.
3 F. K. Gleason, J. Porwoll, J. L. Flippen-Anderson and C. George, *J. Org. Chem.*, 1986, **51**, 1615–1616.
4 F. K. Gleason and J. L. Paulson, *Arch. Microbiol.*, 1984, **138**, 273–277.
5 J. Krumbholz, K. Ishida, M. Baunach, J. E. Teikari, M. M. Rose, S. Sasso, C. Hertweck and E. Dittmann, *Angew. Chem. Int. Ed.*, 2022, **61**, e202204545.
6 X. Yang, Y. Shimizu, J. R. Steiner and J. Clardy, *Tetrahedron Lett.*, 1993, **34**, 761–764.
7 G. D. Brown, H. F. Wong, N. Hutchinson, S. C. Lee, B. K. K. Chan and G. A. Williams, *Phytochem. Rev.*, 2004, **3**, 381–400.
8 S.-C. Lee, G. A. Williams and G. D. Brown, *Phytochemistry*, 1999, **52**, 537–540.
9 H.-F. Wong, G. A. Williams and G. D. Brown, *Phytochemistry*, 2002, **60**, 425–429.
10 S.-C. Lee and G. D. Brown, *J. Nat. Prod.*, 1998, **61**, 29–33.
11 Tsui, Wing-Yan, G. A. Williams and G. D. Brown, *Phytochemistry*, 1996, **43**, 1083–1085.
12 G. D. Brown and H.-F. Wong, *Tetrahedron*, 2004, **60**, 5439–5451.
13 P. M. D'Agostino, C. J. Seel, X. Ji, T. Gulder and T. A. M. Gulder, *Nat. Chem. Biol.*, 2022, **18**, 652–658.
14 C. Greunke, E. R. Duell, P. M. D'Agostino, A. Glöckle, K. Lamm and T. A. M. Gulder, *Metab. Eng.*, 2018, **47**, 334–345.
15 P. M. D'Agostino and T. A. M. Gulder, *ACS Synth. Biol.*, 2018, **7**, 1702–1708.
16 E. R. Duell, P. M. D'Agostino, N. Shapiro, T. Woyke, T. M. Fuchs and T. A. M. Gulder, *Microb. Cell Factories*, 2019, **18**, 32.
17 N. Eusébio, R. Castelo-Branco, D. Sousa, M. Preto, P. M. D'Agostino, T. Gulder and P. Leão, *ACS Synth. Biol.*, 2022, **11**, 3493–3503.
18 X. Ouyang, P. M. D'Agostino, M. Wahlsten, E. Delbaje, J. Jouni, P. Permi, G. Giaini, A. Poso, P. Bartos, T. A. M. Gulder and H. Koistinen, *Org. Biomol. Chem.*, 2023, 4893–4908.
19 E. R. Duell, T. M. Milzarek, M. E. Omari, L. J. Linares-Otoya, T. F. Schäberle, G. M. König and T. A. M. Gulder, *Org. Chem. Front.*, 2020, **7**, 3193–3201.
20 X.-H. Mo, Q.-Y. Pu, T. Lübken, G.-H. Yu, M. Malay, P. M. D'Agostino and T. A. M. Gulder, *Cell Chem. Biol.*, 2024, **31**, 2128-2137.e4.
21 A. Glöckle, S. Schuler, M. Einsiedler and T. A. M. Gulder, *Microb. Cell Factories*, 2025, **24**, 13.
22 J. K. Evers, A. Glöckle, M. Wiegand, S. Schuler, M. Einsiedler and T. A. M. Gulder, *Biotechnol. Bioeng.*, DOI:10.1002/bit.28919.
23 K. H. Liland, *TrAC Trends Anal. Chem.*, 2011, **30**, 827–841.
24 J. Bartel, J. Krumsiek and F. J. Theis, *Comput. Struct. Biotechnol. J.*, 2013, **4**, e201301009.
25 R. Uchida, K. Shiomi, T. Sunazuka, J. Inokoshi, A. Nishizawa, T. Hirose, H. Tanaka, Y. Iwai and S. Omura, *J. Antibiot. (Tokyo)*, 1996, **49**, 886–889.
26 M. Naville, A. Ghuillot-Gaudeffroy, A. Marchais and D. Gautheret, *RNA Biol.*, 2011, **8**, 11–13.
27 M. C. Chambers, B. Maclean, R. Burke, D. Amodei, D. L. Ruderman, S. Neumann, L. Gatto, B. Fischer, B. Pratt, J. Egertson, K. Hoff, D. Kessner, N. Tasman, N. Shulman, B. Frewen, T. A. Baker, M.-Y. Brusniak, C. Paulse, D. Creasy, L. Flashner, K. Kani, C. Moulding, S. L. Seymour, L. M. Nuwaysir, B. Lefebvre, F. Kuhlmann, J. Roark, P. Rainer, S. Detlev, T. Hemenway, A. Huhmer, J. Langridge, B. Connolly, T. Chadick, K. Holly, J. Eckels, E. W. Deutsch, R. L. Moritz, J. E. Katz, D. B. Agus, M. MacCoss, D. L. Tabb and P. Mallick, *Nat. Biotechnol.*, 2012, **30**, 918–920.
28 M. Wang, J. J. Carver, V. V. Phelan, L. M. Sanchez, N. Garg, Y. Peng, D. D. Nguyen, J. Watrous, C. A. Kapono, T. Luzzatto-Knaan, C. Porto, A. Bouslimani, A. V. Melnik, M. J. Meehan, W.-T. Liu, M. Crüsemann, P. D. Boudreau, E. Esquenazi, M. Sandoval-Calderón, R. D. Kersten, L. A. Pace, R. A. Quinn, K. R. Duncan, C.-C. Hsu, D. J. Floros, R. G. Gavilan, K. Kleigrewe, T. Northen, R. J. Dutton, D. Parrot, E. E. Carlson, B. Aigle, C. F. Michelsen, L. Jelsbak, C. Sohlenkamp, P. Pevzner, A. Edlund, J. McLean, J. Piel, B. T. Murphy, L. Gerwick, C.-C. Liaw, Y.-L. Yang, H.-U. Humpf, M. Maansson, R. A. Keyzers, A. C. Sims, A. R. Johnson, A. M. Sidebottom, B. E. Sedio, A. Klitgaard, C. B. Larson, C. A. Boya P, D. Torres-Mendoza, D. J. Gonzalez, D. B. Silva, L. M. Marques, D. P. Demarque, E. Pociute, E. C. O'Neill, E. Briand, E. J. N. Helfrich, E. A. Granatosky, E. Glukhov, F. Ryffel, H. Houson, H. Mohimani, J. J. Kharbush, Y. Zeng, J. A. Vorholt, K. L. Kurita, P. Charusanti, K. L. McPhail, K. F. Nielsen, L. Vuong, M. Elfeki, M. F. Traxler, N. Engene, N. Koyama, O. B. Vining, R. Baric, R. R. Silva, S. J. Mascuch, S. Tomasi, S. Jenkins, V. Macherla, T. Hoffman, V. Agarwal, P. G. Williams, J. Dai, R. Neupane, J. Gurr, A. M. C. Rodríguez, A. Lamsa, C. Zhang, K. Dorrestein, B. M. Duggan, J. Almaliti, P.-M. Allard, P. Phapale, L.-F. Nothias, T. Alexandrov, M. Litaudon, J.-L. Wolfender, J. E. Kyle, T. O. Metz, T. Peryea, D.-T. Nguyen, D. VanLeer, P. Shinn, A. Jadhav, R. Müller, K. M. Waters, W. Shi, X. Liu, L. Zhang, R. Knight, P. R. Jensen, B. Ø. Palsson, K. Pogliano, R. G. Linington, M. Gutiérrez, N. P. Lopes, W. H. Gerwick, B. S. Moore, P. C. Dorrestein and N. Bandeira, *Nat. Biotechnol.*, 2016, **34**, 828–837.
29 P. Shannon, A. Markiel, O. Ozier, N. S. Baliga, J. T. Wang, D. Ramage, N. Amin, B. Schwikowski and T. Ideker, *Genome Res.*, 2003, **13**, 2498–2504.
30 K. Saurav, M. Macho, A. Kust, K. Delawská, J. Hájek and P. Hrouzek, *Folia Microbiol. (Praha)*, 2019, **64**, 645–654.
31 Y. Hirose, Y. Ohtsubo, N. Misawa, C. Yonekawa, N. Nagao, Y. Shimura, T. Fujisawa, Y. Kanesaki, H. Katoh, M. Katayama, H. Yamaguchi, H. Yoshikawa, M. Ikeuchi, T. Eki, Y. Nakamura and M. Kawachi, *DNA Res.*, 2021, **28**, dsab024.